Modified Model of DI Diesel Engine Combustion

Phiphat Bijayendrayodhin
Siridhorn International Institute of Technology,
Thammasat University, Patum Thani 12121, Thailand
Phone (66-2) 986-9009, ext 2211
Email: pbij@siit.tu.ac.th

Abstract

A phenomenological combustion model for the direct-injection, quiescent chamber, diesel engine based on axial division of the fuel spray was modified to enable accurate prediction of exhaust NO_x and particulate emissions. The fuel spray axial divisions were further sub-divided into radial divisions. This allowed the fuel-air concentration to vary from fuel rich at the spray core to fuel lean around the spray periphery

Modification of the air entrainment model was needed for the multi-zone fuel-air distribution since there were air compositional variations in the cylinder. In the model, the air entrainment in the free spray was estimated from momentum conservation equation. The wall jet air entrainment was calculated from the volume of the wall jet based on Poreh's wall jet velocity distribution. The predicted cylinder pressure diagrams were in good agreement with experimental results.

The extended Zeldovich mechanism was used for calculating NO formation using the rate constant recommended by Mellor et al. The modified Hiroyasu's soot production model was used for estimating soot production. Hiroyasu's soot oxidation coefficient was replaced by using the Nagle and Strickland-Constable's oxidation model. The predicted results of emissions were acceptable.

Introduction

Combustion in a direct injection diesel engine takes place in a heterogeneous mixture. The combustion process comprises fuel injection, droplet atomization and distribution, evaporation, fuel-air mixing, fuel-air oxidation, heat transfer and overall conservation of energy. There are two classes of combustion models for this purpose: thermodynamic models and multi-dimension models.

In this study, the model is called the multi-zone or quasi-dimensional model where the fuel sprays and the surrounding air are divided separately into a number of zones. The fuel spray is divided into a large number of zones depending upon the duration of fuel injection.

In this study, Kumar's [1, 2] multi-zone model, in which the fuel spray was only divided into a number of zones along the spray axis, is extended to include radial zones or shells. Thus, the air entrainment in the spray is not only varied in the axial direction, but also in the radial direction. Kumar's model was able to predict cylinder pressure diagrams accurately, compared with results from experiments. However its ability to predict exhaust emissions such as NOx and soot was not good. This is because the spray division was too rough to evaluate the temperature and composition distribution across each axial zone. Moreover, the NO and soot formation models strongly depend on the fuel-air equivalence ratio and temperature of the zones. Therefore, the structure of Kumar's model was modified for estimating the temperature and fuel-air distribution in radial and axial location.

The purpose of this paper is to describe the model and show its performance as an inexpensive tool for predicting emissions from diesel engine combustion.

Spray Division

The composition of fuel-air mixture and temperature in the fuel spray varies with axial and radial positions due to the amount of air entrained into the spray being non-uniform throughout the spray region. Generally, the spray has a rich mixture at its core whilst the mixture is lean at the periphery of the spray [3]. In addition, the fuel-air mixing process controls the fuel oxidation process. Therefore, the temperature of the spray is not uniform but

RECEIVED 4 OCTOBER, 2002
ACCEPTED 16 MAY, 2003

depends on the rate of fuel oxidation. NO and soot prediction models depend on the local equivalence ratio, and temperature.

In Kumar's spray division, the sprays were divided into a zone per crank angle throughout the period of fuel injection, thus the number of zones equals to the injection period in degree crank angle, as shown in Fig 1. In this study, the zone is also subdivided by radius into a number of shells. Each axial zone is subdivided into ten radial shells. The core is arbitrarily set as the first shell. The shell at the periphery of the spray zone is set as the tenth.(Fig. 2)

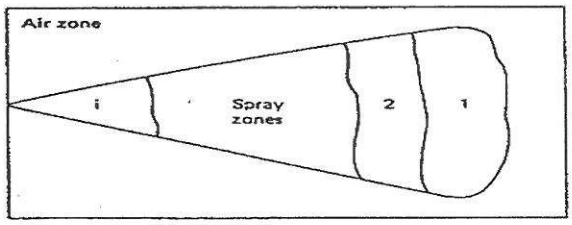

Figure 1 The schematic of Kumar's spray division [1,2].

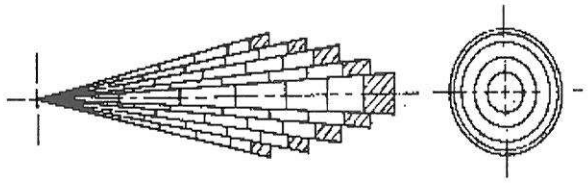

Figure 2 The schematic of Hiroyasu's spray division [4, 5].

Spray Penetration

The velocities of shells in each zone are not equal. The velocity in the outer shell is lower than the inner shell, due to shear stress from the surrounding air. Then the spray penetration of each shell is varied with radical distance from the axis. Hiroyasu et al [4] proposed a spray penetration distribution expression to estimate the penetration of the shell away from the centerline. By implementing Hiroyasu's [4] expression of spray penetration distribution with Kumar's [1] spray tip penetration, the penetration of each shell is estimated. Kumar's spray tip penetration is shown in the following equation:

$$S_P(t) = C_{Sp}\left(\frac{\Delta P}{\rho_a}\right)^{0.25} \nu_f^{0.11} \cdot \tanh t^{0.715} \qquad (1)$$

$$S_L = S_p \cdot \exp(C_{S_L} \cdot (L-1)^2) \qquad (2)$$

$S_p(t)$ = tip penetration, m
ΔP = difference between injection and cylinder pressure, Pa
ν_f = kinematic viscosity of fuel, m^2/s
ρ_a = the ambient density, kg/m^3
C_{Sp} = constant, 0.461
t = time, s
S_L = spray penetration of each shells, m
C_{SL} = -8.557×10^{-3}, from Hiroyasu [3]
L = the arbitrary number, from 1..10, with the center shell as 1.

Spray Air Entrainment

The momentum conservation equation is used to estimate the amount of air entrained. The mass of fuel and the injection velocity is used to calculate the initial momentum. After the start of fuel injection, the spray velocity of each shell for each time step is computed and used for estimating the mass of air entrained.

Wall Jet Penetration

Wall jet penetration expression derived from Poreh et al's [6] wall jet velocity distribution is

$$r_w = 1.141 \cdot \left(H^{0.1} \cdot K^{1/2} \cdot t\right)^{1/2.1} + C_w \qquad (3)$$

$$K = \frac{\pi}{4} \cdot d_e^2 \cdot u_0^2 \qquad (4)$$

$$d_e = \left(\frac{\rho_f}{\rho_a}\right)^{\frac{1}{2}} d_n \qquad (5)$$

We use $d(r_w)/dt = U_{w,max}$, to calculate the wall jet penetration and velocity.

$U_{w,max}$ = the maximum wall jet velocity, m/s
r_w = the wall jet penetration, m
K = the kinematic momentum flux, m^4/s^2

H = the distance of the nozzle tip from the combustion bowl, m

d_e = equivalence nozzle diameter, m

U_0 = the injection velocity, m/s

C_w = the radius from the center of the spray of each shells to the rim of the shell

Next the impact of the spray at the chamber wall is considered. The initial radius of each shell reaching the wall is found from the tangent of the spray angle of that shell with the distance from the nozzle tip to the combustion bowl. This spray angle of the spray is :

$$\alpha = 0.97 \cdot \mu_f^{-0.03} \cdot \rho_f^{0.09} \cdot \rho_a^{0.14} \cdot \Delta P^{0.115} \quad (6)$$

α = semi spray angle of the zone, °

μ_f = dynamic viscosity, N-s/m^2

The following assumptions are made for the spray-wall interaction.

1. Shells that are generated at the same time, are confined within the overall spray angle.
2. The mass of air in a spray zone is equal to the summation of mass of air in its shells
3. The spray path length of the shells to the piston bowl wall equals the distance from the nozzle tip to the wall.
4. The volumes of shells in each zone are distributed according to the modified Hiroyasu's expression, for free sprays until impingement, according to equation 2, but the mass of air entrainment varies with Hiroyasu's expression.
5. The spray cross section is circular.

From the above assumptions the relationship between the core shell volume with the outer volume is obtained by the modified Hiroyasu's expression, as follows:

$$V_{L,int} = \frac{V_{L=1,int}}{C_1} = \frac{\pi}{3} \cdot \left[(B_2)^2 - (B_1)^2 \right] \cdot H^3 \quad (7)$$

$$V_{L,int,total} = V_{L=1,int} \cdot \sum_{L=1}^{10} \left[\frac{1}{C_1} \right] = \frac{\pi}{3} (A_1)^2 \cdot H^3 \quad (8)$$

$$\beta_L = \tan^{-1}\left(\sqrt{A_2} \right) \quad (9)$$

$$A_1 = \tan \alpha$$

$$A_2 = \frac{A_1^2}{C_1 \cdot \sum_{L=1}^{10} \frac{1}{C_1}} + B_1$$

$$B_1 = \tan \beta_{L-1}$$

$$B_2 = \tan \beta_L$$

$$C_1 = \exp(-C_{s_L} \cdot (L-1)^2)$$

β_L = semi spray angle of each shell, °

L = 1..10, degrees

V_L = volume of shell, L = 1...10

$V_{L,total}$ = total volume of the zone, which equals to the summation of the volume of shells in that zone

Thus, the initial radius, C_w, is estimated from the tangent of the distance from the nozzle tip to the bowl with the spray angle of shell.

Wall Jet Air Entrainment

At the time immediately prior to impingement the processes are calculated for the free spray, but the wall jet air entrainment governs the next step. Each shell spreads radially outward after impingement. The incremental volume of each shell in the wall jet changes over the time increment, and is used for estimating the mass of wall jet air entrained. In addition, the initial wall jet volume is calculated from mass conservation at the time of impingement.

The total shell volumes of the wall jet is approximated by the revolution of an area, whose height equals to the wall jet boundary thickness (b_w) and its width equals to the differential value of the wall jet penetration for a time increment ($U_{w,max}$ x Δt). The distance of the impinged jet front from the center of the spray is the wall jet penetration (r_w). The changing volume of each shell is found from the difference in volume between successive time steps. The incremental value of shell volume is multiplied by the air density to estimate the approximate mass of wall jet air entrainment.

The volume of shell (wall jet) at any time, t, is calculated using the following equation.

$$V_{L,t} = 2 \cdot \pi \cdot r_w \cdot b_w \cdot u_{w,mean} \cdot \Delta t \qquad (10)$$

$V_{L,t}$ = volume of shell L, L = 1..10, at time t, m^3

Δt = a time increment, s

$u_{w,mean}$ = mean velocity of wall jet, m/s

b_w = the height of wall jet boundary, m

The relation of δ_w with wall jet penetration and the distance from the nozzle tip to the wall is shown in equation 11 [6].

$$\frac{\delta_w}{r_w} = 0.098\left(\frac{r_w}{H}\right)^{-0.1} \qquad (11)$$

δ_w = characteristic thickness of the wall jet, m

Integrating Poreh's wall jet velocity distribution [6], the following equation is obtained;

$$b_w \cdot u_{w,mean} = 1.047 \cdot u_{w,max} \cdot \delta_w \qquad (12)$$

The mass of wall jet air entrained, $\dot{m}_w$ is defined as;

$$\dot{m}_w = \rho_{air} \cdot (V_{L,t} - V_{L,t-1}) \qquad (13)$$

NO Formation

The NOx formation was derived by Heywood [3] based on the extended Zeldovich mechanism for NO prediction. The extended Zeldovich mechanism consists of the following:

$$O + N_2 \Leftrightarrow NO + N \quad \ldots (A)$$

$$N + O_2 \Leftrightarrow NO + O \quad \ldots (B)$$

$$N + OH \Leftrightarrow NO + H \quad \ldots (C)$$

Heywood derived a single expression of the NO formation by the rate equations from the extended Zeldovich mechanism, with a steady state assumption for N, which results from setting d[N]/dt = 0, in rate equation (A), (B) and (C).

The extended Zeldovich mechanism can be written as a single rate equation for NO. The NO formation expression is shown in the following equation.

$$\frac{d}{dt}[NO] = 2k_1\left\{\frac{1-[NO]^2/K_{12}[O_2][N_2]}{1+k_2/k_3}\right\} \qquad (14)$$

$$k_1 = k_{1f}[O][N_2]$$

$$k_2 = k_{1b}[NO]$$

$$k_3 = k_{2f}[O_2] + k_{3f}[OH]$$

K_{12} = $(k_{1f}/k_{1b}) \times (k_{2f}/k_{2b})$

Subscript 1,2 and 3 refer to equations A, B, C respectively. O, OH, O_2, and N_2 are assumed to be in local thermodynamic equilibrium, specific for each package.

The rate constants, as recommended by Mellor et al [7], are used in the NO formation expression, as shown in the following.

$k_{1,f}$ = $1.63 \times 10^{11} \times \exp[-38{,}095 / T(K)]$

$k_{1,b}$ = $3.5 \times 10^{10} \times \exp[-166 / T(K)]$

$k_{2,f}$ = $2.65 \times 10^{9}\, T \times \exp[-3{,}226 / T(K)]$

$k_{2,b}$ = $5.9 \times 10^{8}\, T \times \exp[-19{,}430 / T(K)]$

$k_{3,f}$ = $7.33 \times 10^{10} \times \exp[-564 / T(K)]$

$k_{3,b}$ = $1.82 \times 10^{11} \times \exp[-24{,}528 / T(K)]$

The unit is m^3/kmol-s.

The rate constant $k_{1,f}$ [7] is the dominant factor that controls the rate of NO formation.

Soot Formation and Oxidation

Hiroyasu's soot production model [3] is used in this study. The model predicts the production of soot mass by a single step competition between the soot formation and oxidation. The Nagle and Strickland-Constable (NSC) oxidation model, which is more realistic prediction, was used to modify Hiroyasu's soot oxidation model.

The NSC oxidation rate coefficient based on the oxidation experiments of carbon graphite in

an O_2 environment over a range of partial pressures. Based on structural similarities, the rates of oxidation of soot and those of pyrographites should be the same. This is a significant simplification. It has proved difficult to follow the oxidation of soot aerosols in flames, and if care is taken to avoid diffusion resistance, studies of bulk samples of pyrographite can then be used as a basis for understanding soot oxidation.

The rate of change of soot mass is equal to the rate of formation subtracted by the rate of oxidation. The soot formation rate is proportional to the mass of unburned vaporized fuel, while the soot oxidation rate is proportional to the soot mass. Hiroyasu soot production model [4, 5] is shown in the following equation.

$$\frac{d}{dt}m_s = \frac{dm_{sf}}{dt} - \frac{dm_{so}}{dt} \qquad (15)$$

The soot formation and oxidation rates are given by the following equations:

$$\frac{dm_{sf}}{dt} = K_f m_{ufv} \qquad (16)$$

m_{sf} = the quantity of soot formation, kg

m_{ufv} = mass of vaporized fuel unburned, kg

m_{so} = the quantity of soot oxidation, kg

K_f = soot formation coefficient, s^{-1}

K_o = soot oxidation coefficient, s^{-1}

Hiroyasu soot formation coefficient is a function of pressure (bar) and the temperature (K) as shown in the following equation.

$$K_f = A_{sf} \cdot P^{0.5} \cdot \exp(-E_{sf}/RT) \qquad (17)$$

A_{sf} = the Arrhenius pre-exponential constant, s^{-1}

P = cylinder pressure, bar

(pressure in Pa / 0.1×10^6 = bar)

E_{sf} = activation energy, 12,500 cal/mole

R = universal gas constant,

1.9858 cal/gmole-K

T = spray package temperature, K

Nagle and Strickland-Constable soot oxidation model is based on the oxidation experiments of carbon graphite in an O_2 environment over a range of partial pressure. The carbon oxidation occurs by two mechanisms whose rates depend on the surface chemistry involving more reactive "A" sites and less reactive "B" sites. The chemical reactions modeled are:

$$A + O_2 \Leftrightarrow A + 2CO \quad \ldots (A)$$

$$B + O_2 \Leftrightarrow A + 2CO \quad \ldots (B)$$

$$A \Leftrightarrow B \quad \ldots (C)$$

By assuming particles are in spherical shape and a uniform size, the first order soot mass proportionality constant coefficient for the Nagle and Strickland-Constable oxidation rate is in the form of soot oxidation coefficient as shown following.

$$K_o = \frac{6}{\rho_s \cdot D_{nom}} \cdot W_{nsc} \qquad (18)$$

K_o = soot oxidation coefficient, s^{-1}

ρ_s = soot density, 2.5 g/cm^3 [8]

D_{nom} = nominal soot particle size,

25×10^{-7} cm [8]

W_{nsc} = a surface mass oxidation rate,

g-carbon/ s-cm^2

Where the proportion of the A sites is:

$$W_{nsc} = \left\{\left(\frac{K_A \cdot P_{O_2}}{1 + K_Z \cdot P_{O_2}}\right) \cdot x + K_B \cdot P_{O_2} \cdot (1-x)\right\} \cdot Mw_c \qquad (19)$$

The rate constants in gmole-carbon/s-cm^2 are shown as follows:

$$x = \frac{P_{O_2}}{P_{O_2} + (K_T / K_B)} \qquad (20)$$

K_A $= 20 \times \exp(-30{,}000 / RT)$

K_B $= 4.46 \times 10^{-3} \times \exp(-15{,}200 / RT)$

K_T $= 1.51 \times 10^{5} \times \exp(-97{,}000 / RT)$

K_Z $= 21.3 \times \exp(4{,}100 / RT)$

R = gas constant, 1.9858 cal/gmole-K

T =spray shell temperature, K

Results and Discussion

An open chamber, naturally aspirated direct injection, four stroke diesel engine was used for this investigation. Its specifications are described in table 1.

TABLE 1. Engine Specification

Engine	PETTER PH1W
Combustion Chamber	Semi-spherical bowl in piston, low swirl
Injector	3 hole type
Injector System	Jerk pump (variable timing)
Bore	87.31 mm
Stroke	110 mm
Swept Volume	0.658 L
Compression Ratio	16.5 : 1
Engine Rating	6 kW at 2000 rev/min
Valve Timing	Inlet – Opens 21 °CA BTDC.
	Closes 42 °CA ATDC
	Exhaust – Open 47 °CA BBDC
	Closes 21 °CA ATDC

The engine was coupled to a DC motor/generator with a Thycon thyristor controller, which could be used for both absorption and generation of power enabling motoring friction losses to be determined.

The engine was equipped to measure crank rotation and with Kistler piezoelectric transducers cylinder and diesel fuel line pressures.

These transducer outputs were fed through signal conditioners to a computer-based data acquisition system. The exhaust gases were analyzed for CO, CO_2, NO_x, HC and particulates (using a previously established correlation with smoke density [2]). The experimental test matrix is shown in table 2.

Natural aspiration tests were chosen for the base model validation against measured cylinder pressure and exhaust NO and particulates. Moreover, oxygen and nitrogen enrichment tests were also included for validation of NO and particulate emissions by comparison with the experimental results.

TABLE 2. Test Matrix of Load and Speed

Speed/Load	No Load	Half Load	Full Load
1250 rev/min	X	X	X
1500 rev/min	X	X	X
1700 rev/min	X	X	X

Cylinder Pressure and Rate of Cylinder Pressure Rise

The cylinder pressure diagrams from the experiment are compared with the diagrams from the modified model. It should be noted that thermal stress effects on the piezoelectric transducer being located in a high velocity region at the edge of the piston bowl were reduced with RTV silicone coated on the surface of the pressure transducer during the experiments.

Figure 3 and figure 4 show the acceptable results of predicted cylinder pressure compared with the results from experiment and Kumar's model. It may be noted that pre-combustion processes in diesel engines are considered to be divided into physical and chemical processes. The physical processes are spray disintegration, droplet formation, fuel evaporation and air entrainment. The chemical process is the chemical reactions between decomposed heavy hydrocarbons and oxygen. These processes occur during the ignition delay period. The nearly accurate predictions of the point of ignition, seen particularly through the match in dP/dt, the cylinder pressure rise rate, is evident that the model handles the pre-combustion processes well as illustrated in figures 3 and 4. The pressure rise rate is related to heat release rate, which depends on the rate of preparation of the air-fuel mixture.

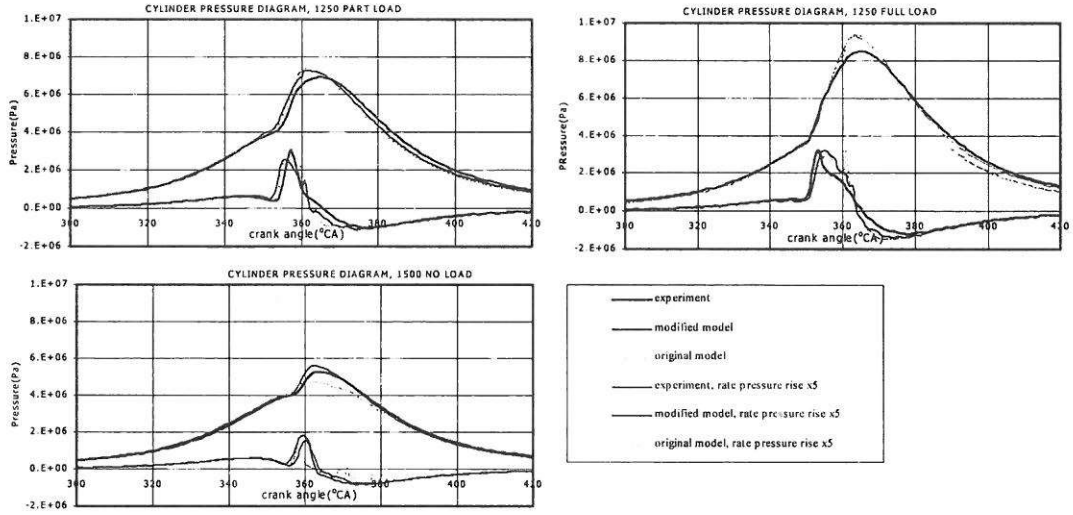

FIG.3. Predicted and measured cylinder pressure and its derivative at moderate speed conditions.

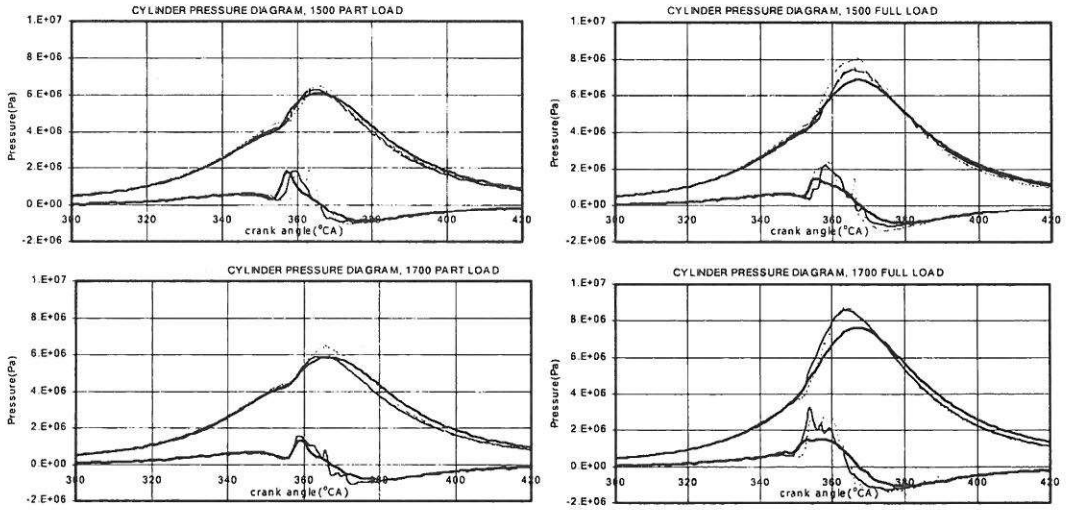

FIG.4. Predicted and measured cylinder pressure and its derivative at moderate speed conditions.

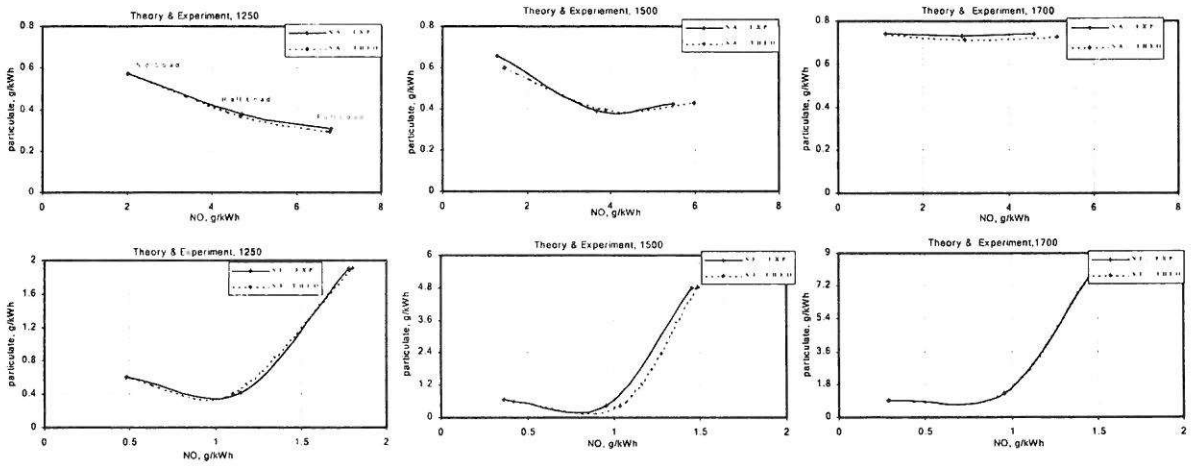

FIG.5. Emission comparison between simulation and experiment, at no-, half- and full-load over the speed range. Normal aspiration (upper), nitrogen dilution (O_2 = 16%) (lower)

NO and Particulate Trade Off Line

The modified model could predict the emissions of nitrogen monoxide and soot production with changing speed, load and oxygen concentration well, as shown in figure 5.

Nitric oxide is the predominant oxide of nitrogen, therefore it is chosen for predicting NO emission. Only the thermal NO was considered in the current model. NO emissions were modeled based upon the widely used extended Zeldovich mechanism. As can been seen, NO formation is reduced when the load is reduced at constant speed because the amount of injected fuel is reduced. Moreover, NO formation is reduced when the speed is increased at the same load.

As a result of the adjusted Arrhenius pre-exponential constant for soot formation for normal air aspiration, the simulated soot production agrees with experimental results. The comparison results in figure 3 show that the model can predict NO and particulate emissions close to the experimental results even with nitrogen dilution of the oxygen at the intake upto 16%. Thus, the Arrhenius pre-exponential constant of soot formation is then used for simulating other areas of study including of oxygen enrichment and the stratification in the cylinder of oxygen and nitrogen layers using the delayed port admission of either the oxygen or the nitrogen component.

Conclusion

Extension of a quasi-dimensional model to include radial as well as axial subdivision of the fuel spray improved the prediction of in-cylinder conditions such as ignition delay and cylinder pressure. In addition, the emissions models performed well in predicting NO and particulate emissions. This validation allowed some confidence in using this model to predict cylinder pressure diagram and emissions.

Acknowledgement

Mr. Bijayendrayodhin performed this work during study for his PhD Thesis supervised by Prof. H.C. Watson at Melbourne University.

References

1. Kumar, S., "Diagnosis of Seed Oils Combustion in a Diesel Engine", Ph.D. Thesis, Department of Mechanical and Manufacturing Engineering, The University of Melbourne, 1986.
2. Desai, R. R., "Oxygen Enrichment of the Diesel Engine", Ph.D. Thesis, Department of Mechanical and Manufacturing Engineering, The University of Melbourne, 1995.
3. Heywood, J. B., "*Internal Combustion Engine Fundamentals*", McGraw-Hill, New York, 1988.
4. Hiroyasu, H., Kadota, T., Arai, M., "Development and Use of a Spray Combustion Modelling to Predict Diesel Engine Efficiency and Pollutant Emissions (Part1, Combustion Modelling)", *Bulletin of the JSME*, vol. 26, No. 214, pp. 569 – 575, April 1983.
5. Yoshizaki, T., Nishida, K. and Hiroyasu, H., "Approach to Low NOx and Smoke Emission Engines by Using Phenomenological Simulation", SAE paper 930612, 1993.
6. Poreh, M., Tsuei, Y. G., and Cermak, J. E., "Investigation of a Turbulent Radial Wall Jet", *Journal of Applied Mechanics*, vol. 34, pp. 457 –463, 1967.
7. Mellor, A. M., Mello, J. P., Duffy, K. P., Easley, W. L. and Faulkner, J. C. "Skeletal Mechanism for NOx chemistry in Diesel Engines", SAE paper 981450, 1998.
8. Hampson, G. J. and Reitz, R. D., "Development of NOx and SOOT Models for Multidimensional Diesel Combustion", EC-Vol.3/FACT-Vol.20, *1995 Joint Power Generation Conference Volume1*, pp. 187 – 198, 1995.